J|A|C|S
ARTICLES
Published on Web 12/23/2006

Ultrafast and Ultraslow Oxygen Atom Transfer Reactions between Late Metal Centers

Kevin C. Fortner, David S. Laitar, John Muldoon, Lihung Pu, Sonja B. Braun-Sand, Olaf Wiest, and Seth N. Brown*

Contribution from the Department of Chemistry and Biochemistry, 251 Nieuwland Science Hall, University of Notre Dame, Notre Dame, Indiana 46556-5670

Received August 7, 2006; E-mail: Seth.N.Brown.114@nd.edu

Abstract: Oxotrimesityliridium(V), $(mes)_3Ir{=}O$ (mes = 2,4,6-trimethylphenyl), and trimesityliridium(III), $(mes)_3Ir$, undergo extremely rapid degenerate intermetal oxygen atom transfer at room temperature. At low temperatures, the two complexes conproportionate to form $(mes)_3Ir{-}O{-}Ir(mes)_3$, the 2,6-dimethylphenyl analogue of which has been characterized crystallographically. Variable-temperature NMR measurements of the rate of dissociation of the μ-oxo dimer combined with measurements of the conproportionation equilibrium by low-temperature optical spectroscopy indicate that oxygen atom exchange between iridium(V) and iridium(III) occurs with a rate constant, extrapolated to 20 °C, of 5×10^7 M^{-1} s^{-1}. The oxotris(imido)osmium(VIII) complex $(ArN)_3Os{=}O$ (Ar = 2,6-diisopropylphenyl) also undergoes degenerate intermetal atom transfer to its deoxy partner, $(ArN)_3Os$. However, despite the fact that its metal−oxygen bond strength and reactivity toward triphenylphosphine are nearly identical to those of $(mes)_3Ir{=}O$, the osmium complex $(ArN)_3Os{=}O$ transfers its oxygen atom *12 orders of magnitude more slowly* to $(ArN)_3Os$ than $(mes)_3Ir{=}O$ does to $(mes)_3Ir$ ($k_{OsOs} = 1.8 \times 10^{-5}$ M^{-1} s^{-1} at 20 °C). Iridium−osmium cross-exchange takes place at an intermediate rate, in quantitative agreement with a Marcus-type cross relation. The enormous difference between the iridium−iridium and osmium−osmium exchange rates can be rationalized by an analogue of the inner-sphere reorganization energy. Both Ir(III) and Ir(V) are pyramidal and can form pyramidal iridium(IV) with little energetic cost in an orbitally allowed linear approach. Conversely, pyramidalization of the planar tris(imido)osmium(VI) fragment requires placing a pair of electrons in an antibonding orbital. The unique propensity of $(mes)_3Ir{=}O$ to undergo intermetal oxygen atom transfer allows it to serve as an activator of dioxygen in cocatalyzed oxidations, for example, acting with osmium tetroxide to catalyze the aerobic dihydroxylation of monosubstituted olefins and selective oxidation of allyl and benzyl alcohols.

Introduction

Oxygen atom transfer reactions (eq 1) are prototypical examples of two-electron inner-sphere redox reactions, with important applications in catalysis in organic synthesis[1] and by metalloenzymes.[2] In general, the net transfer of an oxygen atom requires two steps, with the formation of an intermediate where the oxygen atom is shared between the two redox centers. The thermodynamic requirements of such reactions have been extensively reviewed.[3] Many rate measurements of oxygen atom transfer reactions between transition metal and main group species have been made, although in only a few cases has it been possible to analyze both steps.[4] Kinetic studies of reactions between two different transition metal species have been carried out even more rarely, and so there is little systematic understanding of the factors that affect the rates of intermetal oxygen atom transfer. This situation is in stark contrast to the understanding of outer-sphere single-electron transfer rates provided by Marcus theory, which relates the facility of such reactions to their thermodynamic driving force ($\Delta G°$), the degree to which the bonding environments of the metals must be altered to accommodate the redox change (the inner-sphere reorganization energy, λ_i), and the degree to which the solvent and counterions must reorganize to accommodate the redox change (the outer-sphere reorganization energy, λ_o).[5]

$$M{=}O + X \leftrightarrows M{-}O{-}X \leftrightarrows M + O{=}X \qquad (1)$$

Our desire to better understand the factors that govern intermetal oxygen atom transfer reactions was piqued by our earlier observation[6] that Wilkinson's iridium(V) oxo complex

(1) Wiberg, K. B., Ed. *Oxidation in Organic Chemistry*; Academic Press: New York, 1985.
(2) (a) Spiro, T. G., Ed. *Molybdenum Enzymes*; Wiley: New York, 1985. (b) Hille, R. *Chem. Rev.* **1996**, *96*, 2757−2816. (c) Holm, R. H.; Kennepohl, P.; Solomon, E. I. *Chem. Rev.* **1996**, *96*, 2239−2314.
(3) (a) Holm, R. H. *Chem. Rev.* **1987**, *87*, 1401−1449. (b) Holm, R. H.; Donahue, J. P. *Polyhedron* **1993**, *12*, 571−589.
(4) (a) Moyer, B. A.; Sipe, B. K.; Meyer, T. J. *Inorg. Chem.* **1981**, *20*, 1475−1480. (b) Seymore, S. B.; Brown, S. N. *Inorg. Chem.* **2000**, *39*, 325−332. (c) Bhattacharyya, S.; Chakraborty, I.; Dirghangi, B. K.; Chakravorty, A. *Inorg. Chem.* **2001**, *40*, 286−293.
(5) Lappin, A. G. *Redox Mechanisms in Inorganic Chemistry*. Ellis Horwood: Chichester, 1994; Chapter 2.
(6) Jacobi, B. G.; Laitar, D. S.; Pu, L.; Wargocki, M. F.; DiPasquale, A. G.; Fortner, K. C.; Schuck, S. M.; Brown, S. N. *Inorg. Chem.* **2002**, *41*, 4815−4823.

10.1021/ja065713h CCC: $37.00

$(mes)_3Ir{=}O$ (mes = 2,4,6-trimethylphenyl, mesityl)[7] undergoes degenerate intermetal oxygen atom transfer with trimesityliridium(III)[8] on the NMR time scale at room temperature. Here we report a quantitative study of this exceptionally fast oxygen atom transfer reaction. In particular, through measurements of the self-exchange rates and the rates and equilibria in cross-exchange reactions with the Os(VI)/Os(VIII)═O couple $(ArN)_3Os/(ArN)_3OsO$ (Ar = 2,6-diisopropylphenyl),[9] we can for the first time apply the Marcus cross-relation to oxygen atom transfer reactions.

Experimental Section

General Methods. Except as noted, all weighings were carried out on the benchtop and all other procedures and kinetics measurements were carried out in an inert atmosphere using standard glove box and vacuum line techniques. Dichloromethane and $CHFCl_2$ (Freon-21, Aldrich) were dried over 4 Å molecular sieves, followed by CaH_2. Benzene was dried over Na. Triphenylphosphine, tri-*o*-tolylphosphine, and other reagents used to synthesize the metal complexes were commercially available and were used without further purification. The quinuclidine adduct of osmium tetroxide, $(C_7H_{13}N)OsO_4$, was isolated as described by Griffith.[10] The iridium oxo complex $(mes)_3Ir{=}O$[6,7] and the osmium complexes $(ArN)_3Os$ and $(ArN)_3Os{=}O$ (Ar = 2,6-diisopropylphenyl)[9b] were prepared using literature procedures.

NMR spectra were measured on a Varian VXR-300 or VXR-500 FT-NMR spectrometer. Temperatures below room temperature were calibrated using the separation between the ^{1}H NMR peaks of neat CH_3OH with 0.03 vol % added aqueous HCl.[11] Low-temperature optical spectra were measured using an Ocean Optics spectrophotometer equipped with a fiber optic immersion probe with a 0.2 cm path length.

Measurement of Conproportionation of $(mes)_3Ir$ and $(mes)_3Ir{=}O$ by Visible Spectroscopy. In a typical run, 5.0 mg of $O{=}Ir(mes)_3$ and 0.3 mg of P(*o*-tol)$_3$ (0.13 equiv) were weighed into an NMR tube. Dry CD_2Cl_2 (0.5 mL) was vacuum transferred into the tube, which was then sealed with a Teflon valve. As the reaction proceeds, the P(*o*-tol)$_3$ is oxidized to O═P(*o*-tol)$_3$, generating a mixture of $O{=}Ir(mes)_3$ and $Ir(mes)_3$. When it had been determined by NMR that all of the P(*o*-tol)$_3$ had reacted, the tube was taken into a glove box, poured into a 10 mL volumetric flask, and diluted to 10 mL with $CHFCl_2$ precooled to −90 °C. The solution was poured into a 25 mL two-neck flask into which were inserted a thermocouple and a UV/vis immersion probe with a 2 mm path length. The temperature of the solution was lowered to −140 °C in a cold well in the glove box using liquid nitrogen as the coolant. The solution was allowed to warm up slowly with continuous swirling to maintain a uniform temperature throughout the solution, and the optical spectrum from 450 to 900 nm was recorded between −140 °C and −30 °C.

The optical spectra of pure $O{=}Ir(mes)_3$ and $Ir(mes)_3$ were measured separately and used to determine the concentrations $[Ir(mes)_3]_0$ and $[O{=}Ir(mes)_3]_0$ in the flask used for the equilibrium constant measurement at −30 °C, at which temperature $[(mes)_3Ir{-}O{-}Ir(mes)_3]$ is negligible. This was done by fitting the entire optical spectrum from 450 to 850 nm of the solution at −30 °C to a linear combination of the spectra of pure $O{=}Ir(mes)_3$ and $Ir(mes)_3$. The Ir(III)/Ir(V) ratios determined by this method agreed within a few percent with those measured by ^{1}H NMR measurements of the CD_2Cl_2 solutions after reduction with phosphine. Absorbances were corrected for temperature using the volume contraction of the $CHFCl_2$ with decreasing temperature ($d\rho/dt = -0.00242$ g mL^{-1} K^{-1} and ρ at 293 K = 1.3783 g mL^{-1}).[12]

Three runs, with total iridium concentrations ranging from 0.51 to 1.18 mM and mole fractions of Ir(III) at room temperature ranging from 0.30 to 0.94, were analyzed over the temperature range −40 to −140 °C. Concentrations of the three species $(mes)_3Ir$, $(mes)_3Ir{-}O{-}Ir(mes)_3$, and $(mes)_3Ir{=}O$ were calculated using the measured total iridium concentration and the measured ratio of oxygen to iridium and the conproportionation K_{eq}, which was calculated using $\Delta H°$ and $\Delta S°$ as adjustable parameters. Theoretical values for the absorbance at 513 nm were calculated using these concentrations, the measured extinction coefficients for $(mes)_3Ir$ (920 M^{-1} cm^{-1}) and $(mes)_3Ir{=}O$ (1020 M^{-1} cm^{-1}), and the extinction coefficient for $(mes)_3Ir{-}O{-}Ir(mes)_3$ as a third adjustable parameter. The three adjustable parameters were allowed to vary, and the sum of $[(A_{calcd} - A_{obsd})^2]/A_{calcd}$ was minimized using Solver in Microsoft Excel.[13] Optimized values for the parameters were $\Delta H° = -5.14 \pm 0.13$ kcal/mol, $\Delta S° = -15.2 \pm 0.7$ cal/mol K, and ϵ_{513} of $(mes)_3Ir{-}O{-}Ir(mes)_3 = 25\,400 \pm 300$ M^{-1} cm^{-1}, with estimated errors calculated as described in the literature.[14]

Preparation of $(2,6\text{-}Me_2C_6H_3)_3Ir{=}O$. This compound has been described briefly in the literature.[7] It was prepared by the same procedure used to prepare $(mes)_3Ir{=}O$,[6] substituting 2,6-dimethylphenylmagnesium bromide (Aldrich) for mesitylmagnesium bromide. After purification by repeated chromatography on silica gel, eluting with 2% Et_2O/hexane, followed by crystallization from acetonitrile/water, $(2,6\text{-}Me_2C_6H_3)_3Ir{=}O$ was isolated as dark blue crystals in 3.3% yield. ^{1}H NMR (C_6D_6): δ 2.50 (s, 18H, C*H*$_3$); 6.49 (t, 7 Hz, 3H, *p*-Ar*H*), 6.95 (d, 7 Hz, 6H, *m*-Ar*H*). $^{13}C\{^1H\}$ NMR (C_6D_6): δ 28.94 (*C*H$_3$), 127.80 (*para*), 130.43 (*meta*), 132.56 (*ortho*), 147.58 (*ipso*). UV−vis (CH_2Cl_2): $\lambda_{max} = 616$ nm, $\epsilon = 2040$ M^{-1} cm^{-1}. IR (evaporated film, cm^{-1}): 3049 (w), 2958 (w), 2922 (w), 2849 (w), 1442 (s), 1374 (w), 1234 (w), 1166 (w), 1025 (w), 844 (m), 763 (m), 667 (w). Anal. Calcd for $C_{24}H_{27}IrO$: C, 55.04; H, 5.21. Found: C, 55.26; H, 5.11.

X-ray Crystallography of $(2,6\text{-}Me_2C_6H_3)_3Ir{-}O{-}Ir(2,6\text{-}Me_2C_6H_3)_3{\cdot}CD_2Cl_2$. A solution of $(2,6\text{-}Me_2C_6H_3)_3Ir{=}O$ in CD_2Cl_2 was treated with a substoichiometric amount of P(*o*-tol)$_3$. Very dark brown crystals of the μ-oxo complex grew when a sealed NMR tube containing this solution was allowed to stand in a −20° freezer for several weeks. A $0.4 \times 0.3 \times 0.3$ mm^3 crystal was removed from the tube and placed in inert oil and transferred to the tip of a glass fiber in the cold N_2 stream of a Bruker Apex CCD diffractometer ($T = -173$ °C). Data were reduced, correcting for absorption and decay, using the program SADABS. The crystal was cubic, and its space group was determined to be $Pa\bar{3}$ from the systematic absences. The structure was solved using Patterson methods, which located the iridium atom (on the crystallographic $\bar{3}$ axis) and oxygen atom (on the inversion center). The single crystallographically unique aryl group and the dichloromethane molecule (whose carbon atom was disordered about an inversion center, with the two chlorine atoms located on the $\bar{3}$ axis) were located on difference Fourier maps. Hydrogens were placed in calculated positions. Final full-matrix least-squares refinement on F^2 converged at $R1 = 0.0156$ for 2024 reflections with $F_o > 4\sigma(F_o)$, $R1 = 0.0177$ for all 2186 unique reflections ($wR_2 = 0.0385$, 0.0396, respectively). All calculations used SHELXTL (Bruker Analytical X-ray Systems), with scattering factors and anomalous dispersion terms taken from the literature.[15]

Measurement of $(mes)_3Ir{-}O{-}Ir(mes)_3$ Dissociation by ^{1}H NMR Line shape Analysis. Solutions of $(mes)_3Ir{=}O$ in CD_2Cl_2 were partially

(7) Hay-Motherwell, R. S.; Wilkinson, G.; Hussain-Bates, B.; Hursthouse, M. B. *Polyhedron* **1993**, *12*, 2009−2012.
(8) Hay-Motherwell, R. S.; Wilkinson, G.; Hussain-Bates, B.; Hursthouse, M. B. *J. Chem. Soc., Dalton Trans.* **1992**, 3477−3482.
(9) (a) Anhaus, J. T.; Kee, T. P.; Schofield, M. H.; Schrock, R. R. *J. Am. Chem. Soc.* **1990**, *112*, 1642−1643. (b) Schofield, M. H.; Kee, T. P.; Anhaus, J. T.; Schrock, R. R.; Johnson, K. H.; Davis, W. M. *Inorg. Chem.* **1991**, *30*, 3595−3604.
(10) Cleare, M. J.; Hydes, P. C.; Griffith, W. P.; Wright, M. J. *J. Chem. Soc., Dalton Trans.* **1977**, 941−944.
(11) Gordon, A. J.; Ford, R. A. *The Chemist's Companion*; John Wiley & Sons: New York, 1972; p 303.
(12) Riddick, J. A.; Burger, W. B.; Sakano, T. K. *Organic Solvents: Physical Properties and Methods of Purification*, 4th ed.; John Wiley & Sons: New York, 1986; pp 490, 560.
(13) Harris, D. C. *J. Chem. Educ.* **1998**, *75*, 119−121.
(14) de Levie, R. *J. Chem. Educ.* **1999**, *76*, 1594−1598.
(15) *International Tables for Crystallography*; Kluwer Academic Publishers: Dordrecht, The Netherlands, 1992; Vol. C.

reduced by allowing the solution to stand at room temperature in a sealed NMR tube for several days or by the addition of substoichiometric amounts of PPh_3. The composition of the solutions was analyzed by integration of the spectra at −110 °C (where the species give separate resonances) or by measurement of the chemical shifts at room temperature (where Ir(V) and Ir(III) give rise to weighted-average resonances). ^{1}H NMR spectra were recorded between −80° and −110 °C on a Varian VXR-500 NMR spectrometer. The line shape of the *para*-methyl region was analyzed using the program *g*NMR[16] to generate calculated lineshapes and superimpose them on the observed spectra, with optimization of the fit as a function of k_{diss} performed manually. The spectra were generally simulated assuming that the ratio of the concentrations of the two major iridium-containing species ($(mes)_3Ir{-}O{-}Ir(mes)_3$ and either $(mes)_3Ir{=}O$ or $(mes)_3Ir$) was as determined in the −110 °C spectrum and the concentration of the minor species ($Ir(mes)_3$ if deoxygenation was <50% complete, $(mes)_3Ir{=}O$ if deoxygenation was >50% complete) was negligible. Achieving satisfactory agreement of the chemical shift of the coalesced peaks in the higher-temperature spectra did sometimes require including small amounts of the minor species in the calculation, but never more than 5% of the total iridium concentration. Values of k_{diss} from different runs varied by <15% from the mean values, with no systematic deviations based on whether the solution was generated by autogenous reduction or by addition of PPh_3, or whether $(mes)_3Ir{=}O$ or $(mes)_3Ir$ was the major species exchanging with $(mes)_3Ir{-}O{-}Ir(mes)_3$. Activation parameters were calculated by plotting $\ln(k_{diss}/T)$ vs $1/T$ in the range 170−193 K.

Kinetics of Reduction of $(ArN)_3Os{=}O$ with PPh_3. Solutions of $(ArN)_3Os{=}O$ were prepared in the drybox in dichloromethane (room temperature) or 1,2-dichlorobenzene (variable-temperature) in 1 cm quartz cells fitted with septum caps. The cells were inserted into the multicell transport block of a Beckman DU-7500 diode array spectrophotometer. The temperature was regulated by a thermostatted water/ethylene glycol mixture circulated through the cell block and was measured by a thermocouple inserted in the cell block. Solutions were allowed to equilibrate for 10 min at the desired temperature, and reactions were initiated by injecting 20−50 equiv of PPh_3 dissolved in a small volume of solvent. Reactions were monitored by measuring the decrease in absorbance at 610 nm. Pseudo-first-order rate constants were obtained from the slopes of plots of $\ln(A - A_f)$ vs time, which were linear over >4 half-lives. The observed pseudo-first-order rate constants were found to depend linearly on $[PPh_3]$ in the range 0.002−0.010 M in CH_2Cl_2 at room temperature. Activation parameters were calculated from reactions measured in 1,2-dichlorobenzene by plotting $\ln(k_{OsP}/T)$ vs $1/T$ over the range 288.6−330.6 K.

Preparation of $(Ar_DN)_3Os$ (Ar_D = 4-Deuterio-2,6-diisopropylphenyl). A sample consisting of 10 g of 2,6-diisopropylaniline (Acros) was washed twice with 1 mL of D_2O (Cambridge Isotope Laboratories). The aniline was then placed into a 500 mL glass bomb with 100 g of CH_3OD (Aldrich) and 8 mL of concentrated DCl in D_2O (Aldrich). The bomb was sealed, and the mixture was heated for 5 d at 60 °C. The solvent was removed in vacuo and the solid was dissolved in water and rendered basic with sodium carbonate. The solution was extracted three times with ether, and the organic phases were collected. The ether solution was dried with magnesium sulfate and concentrated in vacuo to give 2,6-diisopropylaniline enriched with deuterium at the para position. Using the deuterium-labeled aniline as a starting material, labeled Ar_DNCO[17] and $Os(NAr_D)_3$[9b] were prepared using literature procedures for the corresponding protio compounds. Mass spectral analysis of the parent ion envelope $Os(NAr_D)_3$ was consistent with 82% deuteration of the aryl ligands; ^{1}H NMR indicated that only the para position of the aryl groups contained deuterium. EI-MS (parent ion only; observed, calculated relative intensities in parentheses): *m*/z 714 (9.6, 10.2), 715 (26.2, 27.3), 716 (60.7, 59.6), 717 (84.4, 83.4), 718 (88.9, 88.9), 719 (74.8, 75.6), 720 (100, 100.1), 721 (34.8, 35.8), 722 (6.7, 6.9).

Kinetics of Exchange Between $Os(NAr_D)_3$ and $O{=}Os(NAr)_3$. Reaction mixtures were prepared by weighing in the drybox 6−15 mg each of $O{=}Os(NAr)_3$ and deuterium-enriched $Os(NAr_D)_3$ (Ar = 2,6-diisopropylphenyl) into an NMR tube sealed to a ground glass joint. The solids were dissolved in dry C_6D_6, and the tube was flame-sealed under a vacuum. ^{1}H NMR spectra were taken every day or two as the mixture was allowed to react at 20 °C, and the integrals for the protons in the para positions of the aromatic imido groups for each compound ($O{=}Os(NAr)_3$, δ 6.89 ppm, $Os(NAr)_3$, δ 7.35 ppm) were measured. The fraction of osmium(VI) in the mixture was determined from the peaks for the $(CH_3)_2CH{-}Ar$ septets ($O{=}Os(NAr)_3$, δ 3.48 ppm, $Os(NAr)_3$, δ 3.86 ppm) and remained constant at about 0.5 throughout the course of each reaction.

Kinetics were analyzed according to standard McKay exchange kinetics, with k_{obsd} determined from the slope of the plot of ln{[Os(VI)]/[total Os] − [unlabeled Os(VI)]/[total unlabeled Os]} vs time.[18] These plots curved significantly after ∼1 half-life, apparently due to autocatalysis. The k_{obsd} values determined over the first half-life were reproducible and were proportional to the total osmium concentration. The bimolecular rate constant was averaged over those observed in seven independent runs.

For two of these runs, the EI mass spectra of two mixtures of $O{=}Os(NAr)_3$ and deuterium-labeled $Os(NAr)_3$ dissolved in C_6D_6, which had undergone complete isotopic scrambling as determined by ^{1}H NMR, were acquired. The isotope envelope of the $Os(NAr)_3$ parent ion (*m*/*z* = 714−722) was fit using a combination of the d^0, d^1, d^2, and d^3 isotopomers using a locally written program.[19]

Measurement of K_{eq} for $(mes)_3Ir{=}O + Os(NAr)_3 \leftrightarrows Ir(mes)_3 + O{=}Os(NAr)_3$. $O{=}Ir(mes)_3$ (1.75 mg) and $Os(NAr)_3$ (Ar = 2,6-diisopropylphenyl) (10.0 mg) were mixed in an NMR tube sealed to a ground glass joint and dissolved in CD_2Cl_2 in the drybox. The tube was attached to a needle valve, evacuated at low temperature, and flame-sealed. The solution was allowed to react at room temperature for a few minutes until the system reached equilibrium. The tube was inserted into an NMR probe, and the ^{1}H NMR spectrum was recorded. The sample was cooled in the probe of the NMR spectrometer, and spectra were recorded at temperatures from room temperature to −30 °C at 5° intervals, allowing sufficient time at each temperature for the solution to reach equilibrium. The ratio $[O{=}Os(NAr)_3]/[Os(NAr)_3]$ was determined at each temperature by measuring the relative integrals of the isopropyl methine resonances. The ratio $[Ir(mes)_3]/[O{=}Ir(mes)_3]$ was determined from the chemical shift of the aromatic H compared to its position in the spectra of authentic samples of $(mes)_3Ir$ and $(mes)_3Ir{=}O$ at the same temperature. (Formation of $(mes)_3Ir{-}O{-}Ir(mes)_3$ is negligible at these temperatures and concentrations.)

Kinetics of $(mes)_3Ir{=}O + Os(NAr)_3 \rightarrow Ir(mes)_3 + O{=}Os(NAr)_3$. Freshly prepared solutions of $O{=}Ir(mes)_3$ and $Os(NAr)_3$ in dry, deoxygenated CD_2Cl_2 were mixed under nitrogen in an NMR tube sealed to a ground glass joint and cooled to −78 °C. The NMR tube was evacuated and flame-sealed, and the solution was kept at −78 °C until it was inserted in the NMR probe, which was precooled to the desired temperature (−30 to −70 °C). The reaction was monitored by measuring the change in the chemical shift of the mesityl aromatic and *ortho*-CH_3 resonances over time. Since chemical exchange between $O{=}Ir(mes)_3$ and $Ir(mes)_3$ is rapid on the NMR time scale at these temperatures, a single set of mesityl resonances is seen for mixtures of $O{=}Ir(mes)_3$, $Ir(mes)_3$, and $(mes)_3Ir{-}O{-}Ir(mes)_3$, and the peak positions shift upfield as the iridium is deoxygenated. In order to avoid precipitation of the sparingly soluble μ-oxo complex, the reactions were conducted using dilute solutions of iridium (∼ 1.5 mg/0.6 mL) and

(16) Budzelaar, P. H. M. *gNMR*, v. 3.5.6.; Cherwell Scientific Publishing: 1996.
(17) Knoelker, H.; Braxmeier, T.; Schlechtingen, G. *Angew. Chem., Int. Ed. Engl.* **1995**, *34*, 2497−2500.
(18) Espenson. J. H. *Chemical Kinetics and Reaction Mechanisms*; McGraw-Hill Inc.: New York, 1995.
(19) Brown, S. N.; Mayer, J. M. *Inorg. Chem.* **1992**, *31*, 4091−4100.

were only monitored for the first 10−20% of reaction. Over this range of reaction, the chemical shift changes are linear with time. Second-order rate constants for this initial portion of the reaction were calculated from the slope of these curves, $\partial(\delta)/\partial t$, according to eq 2:

$$k_{\mathrm{IrOs}} = \frac{\partial(\delta)/\partial t}{[\mathrm{Os}]} \cdot \frac{1 + K[\mathrm{Ir}]}{\delta_{\mathrm{Ir(III)}} + 2K[\mathrm{Ir}]\delta_{\mathrm{IrOIr}} - (1 + K[\mathrm{Ir}])\delta_{\mathrm{Ir{=}O}}} \quad (2)$$

where K is the equilibrium constant for the conproportionation of $(mes)_3Ir$ and $(mes)_3Ir{=}O$ calculated from the thermodynamic parameters measured by optical spectroscopy in $CHFCl_2$ and $\delta_{\mathrm{Ir(III)}}$, δ_{IrOIr}, $\delta_{\mathrm{Ir{=}O}}$ are the chemical shifts of the resonances for pure $(mes)_3Ir$, $(mes)_3Ir{-}O{-}Ir(mes)_3$, and $(mes)_3Ir{=}O$, respectively, measured at (or in the case of $(mes)_3Ir{-}O{-}Ir(mes)_3$, extrapolated to) the temperature of the kinetics run. Concentrations of iridium and osmium were corrected for thermal contraction of the solvent.[12] Since the chemical shifts for the μ-oxo complex can only be measured over a very narrow range of temperatures (−100 to −110 °C), this extrapolation is likely to be rather imprecise. However, because the chemical shifts of the μ-oxo complex are close to the average of the shifts of the iridium(III) and iridium(V) complexes, and because the mole fraction of iridium(IV) is small at these concentrations and temperatures, the calculated rate constants are relatively insensitive to the treatment of the μ-oxo complex, with calculated rate constants differing by no more than 10% from those where the formation of the μ-oxo complex is completely neglected. Results from the shifts of the aromatic hydrogens agreed with those measured from the *o*-CH_3 resonances, and second-order rate constants calculated from eq 2 were independent of $[Os(NAr_3)]$ in the range 0.007−0.016 M. Activation parameters were obtained from a plot of $\ln(k/T)$ vs $1/T$.

DFT Calculations on Iridium and Osmium Complexes. Calculations were performed on model complexes with the mesityl groups in the iridium complexes and the 2,6-^{i}Pr$_2$C$_6$H$_3$ groups in the osmium complexes replaced by methyl groups. All structures were optimized using the hybrid B3LYP method, which has been successfully used in a number of studies involving transition metal complexes.[20] A 6-311+G** basis set was used for the carbon, hydrogen, and oxygen atoms, while an SDD basis set was used on the iridium and osmium atoms. Stationary points were characterized by harmonic frequency analysis. Thermochemical corrections to the reported energies were calculated from the harmonic frequency analysis for a temperature of 293 K and a pressure of 1 atm, using a scaling factor of 0.9614.[21] All calculations were performed using the G98[22] and G03[23] series of programs. The Kohn−Sham orbital[24] representations were created in Molden using a contour value of 0.05.

Aerobic Dihydroxylations with $(mes)_3Ir{=}O/(C_7H_{13}N)OsO_4$. Representative Procedure: Dihydroxylation of 1-Octene. Into a screw-capped NMR tube in the air were added $(C_7H_{13}N)OsO_4$ (2.0 mg, 5.5 μmol, 20 mol %), $(mes)_3Ir{=}O$ (3.1 mg, 5.5 μmol, 20 mol %), 1-octene (4.3 μL, 0.027 mmol), and dimethyl terephthalate as an internal standard (1.0 mg, 5.2 μmol) and 0.5 mL of THF-d_8/2% D_2O. The NMR tube was rapidly shaken. The reaction was monitored by NMR and was complete in a week.

Enantioselective Aerobic Dihydroxylation of 1-Octene with $(mes)_3Ir{=}O/OsO_4/(DHQD)_2PHAL$. Into a vial were added OsO_4 (2.5 mg, 9.8 μmol), $(DHQD)_2PHAL$ (Aldrich, 27 mg, 0.035 mmol), and 1 mL of THF-d_8. Into a screw-capped NMR tube were added $(mes)_3Ir{=}O$ (3.1 mg, 5.5 μmol) and 1-octene (4.3 μL, 0.027 mmol). After shaking, 0.5 mL of the $(DHQD)_2PHAL$/osmium solution was added to the NMR tube. Upon completion of the reaction (determined by NMR), the reaction mixture was diluted with Et_2O (8 mL), washed with saturated aqueous sodium sulfite to remove the metals, and dried over $MgSO_4$. After the solvent was removed on the rotary evaporator, the diol was filtered through a small plug of silica gel using EtOAc/hexane (1:1) to give pure 1,2-octanediol. The two enantiomers were separated by chiral GC (J&W Scientific 112−2532, Cyclodex B; injection temperature 250 °C, detector temperature 300 °C, oven temperature 75 °C for 10 min followed by 2 °C/min to 145 °C for 5 min; retention times = 42.6 and 42.9 min).

Representative Procedure for the Oxidation of Benzylic and Allylic Alcohols: Oxidation of Benzyl Alcohol. Into a 2.5 mL screw-capped vial was added a solution of $(mes)_3Ir{=}O$ (4.5 mg, 7.9 μmol, 1 mol %) and benzyl alcohol (82 μL, 0.79 mmol) in 0.4 mL of THF. In an NMR tube, the osmium reagent was generated by adding allyl ethyl ether (12.0 μL, 0.106 mmol, 13.2 mol %) to a suspension of $(quinuclidine)OsO_4$ (5.8 mg, 0.016 mmol, 2 mol %) in 0.1 mL of THF. After allowing this osmium-containing solution to stand for 40 s after addition of the alkene, the solution containing the substrate and iridium was added to the NMR tube. Oxygen gas, presaturated with THF by passing it through a gas dispersion tube in a 100 mL two-neck flask filled with THF, was admitted to the screw-cap NMR tube with a septum cap using a needle. Oxygen was bubbled through the reaction mixture at a moderate rate (~3 bubbles/s) and vented through a mineral oil bubbler. The reaction was complete in 3 days.

Results

Conproportionation of $(mes)_3Ir{=}O$ and $(mes)_3Ir$. Earlier we reported that solutions containing mixtures of Wilkinson's homoleptic trimesityliridium(III), $(mes)_3Ir$ (mes = 2,4,6-trimethylphenyl),[8] and oxotrimesityliridium(V), $(mes)_3Ir{=}O$,[7] display only a single set of mesityl resonances in the ^{1}H NMR at room temperature.[6] This is due to fast intermolecular oxygen atom transfer between iridium(V) and iridium(III) leading to chemical exchange of the two types of mesityl group (eq 3). Given the differences in chemical shift between $(mes)_3Ir{=}O$ and $(mes)_3Ir$ and the fact that only fairly sharp coalesced signals are seen at room temperature, this exchange must take place with $k_{\mathrm{IrIr}} > 4 \times 10^5\ \mathrm{M^{-1}\ s^{-1}}$.

$$(mes)_3Ir{=}O + Ir(mes)_3 \leftrightarrows (mes)_3Ir + O{=}Ir(mes)_3 \quad (3)$$

A logical intermediate in this oxygen atom transfer reaction is the iridium(IV) μ-oxo complex $(mes)_3Ir{-}O{-}Ir(mes)_3$. Results of the earlier study[6] suggest that this conproportionation product is not present in significant concentrations at ambient temperatures. In particular, $(mes)_3Ir{=}O$ is deoxygenated by oxygen atom acceptors such as triphenylphosphine or triphenylarsine in reactions which show clean pseudo-first-order kinetics (in the presence of excess reducing agent) over the entire course of the reaction. Substantial amounts of conproportionation would imply that the reaction would slow as $(mes)_3Ir$ bound to the oxo complex $(mes)_3Ir{=}O$, except in the unlikely event that the μ-oxo complex were more readily deoxygenated than the terminal oxo complex.

Conproportionation is important at lower temperatures, however, as indicated by color changes when mixtures of $(mes)_3Ir{=}O$ and $(mes)_3Ir$ are cooled. Solutions of neither blue-green $(mes)_3Ir{=}O$ nor yellow-brown $(mes)_3Ir$ are thermochromic, and optical spectra taken at room temperature of green solutions containing mixtures of the two compounds are simple

(20) (a) Koch, W.; Holthausen, M. C. *A Chemist's Guide to Density Functional Theory*; Wiley-VCH: Weinheim, 2000. (b) Cundari, T. R. *Computational Organometallic Chemistry*; Marcel-Dekker: New York, 2001. (c) Niu, S.; Hall, M. B. *Chem. Rev.* **2000**, *100*, 353−405.
(21) Scott, A. P.; Radom, L. *J. Phys. Chem.* **1996**, *100*, 16502−16513.
(22) Frisch, M. J., et al. *Gaussian 98*; Gaussian, Inc.: Wallingford, CT, 1998.
(23) Frisch, M. J., et al. *Gaussian 03*, revision C.01; Gaussian Inc.: Wallingford, CT, 2004.
(24) For a discussion of the relationship of Kohn−Sham and Hartree−Fock orbitals, see: Stowasser, R.; Hoffmann, R. *J. Am. Chem. Soc.* **1999**, *121*, 3414−3420.

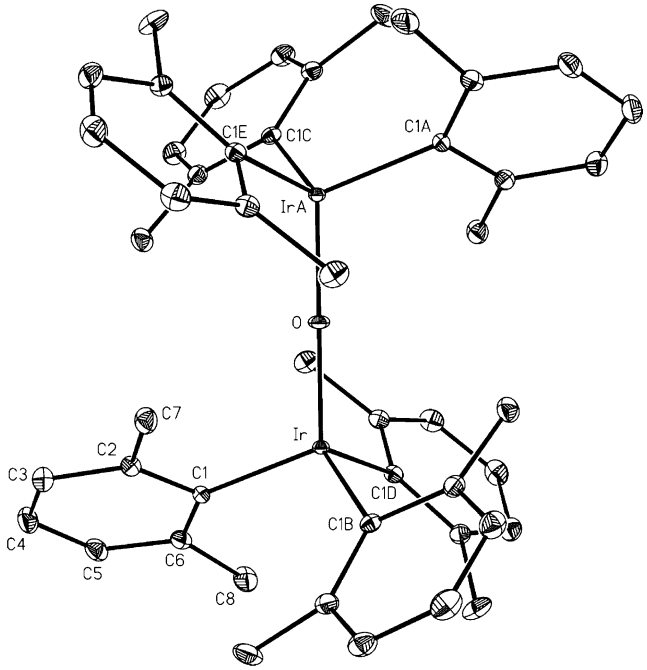

Figure 1. SHELXTL plot (50% ellipsoids) of $(2,6\text{-}Me_2C_6H_3)_3Ir{-}O{-}Ir(C_6H_3\text{-}2,6\text{-}Me_2)_3$.

Table 1. Crystallographic Details for $(2,6\text{-}Me_2C_6H_3)_3Ir{-}O{-}Ir(C_6H_3\text{-}2,6\text{-}Me_2)_3{\cdot}CD_2Cl_2$

empirical formula	$C_{49}H_{54}D_2Cl_2Ir_2O$
FW	1118.31
temperature (K)	100(2)
λ	0.710 73 Å (Mo Kα)
crystal class	cubic
space group	$Pa\bar{3}$
total data collected	51 216
no. of indep reflns.	2186
a (Å)	16.2538(3)
V (Å^3)	4294.03(14)
Z	4
calcd ρ (g/cm^3)	1.730
cryst size (mm^3)	0.4 × 0.3 × 0.3
μ (mm^{-1})	6.352
no. of refined parameters	104
R indices [$I > 2\sigma(I)$][a]	$R1 = 0.0156$, $wR2 = 0.0385$
R indices (all data)[a]	$R1 = 0.0177$, $wR2 = 0.0396$
GOF on F^2	1.082

[a] $R1 = \Sigma||F_o| - |F_c||/\Sigma|F_o|$; $wR2 = (\Sigma[w(F_o^2 - F_c^2)^2]/\Sigma w(F_o^2)^2)^{1/2}$.

superpositions of the optical spectra of the two constituents. However, when dichloromethane solutions are cooled to well below room temperature, a color change from green to dark brown takes place. If the solutions are allowed to stand at low temperature, a dark brown microcrystalline precipitate forms. Both the precipitation and the color change are reversed on warming the sample.

By allowing a partially reduced sample of the 2,6-dimethylphenyl analogue $(2,6\text{-}Me_2C_6H_3)_3Ir{=}O$[7] to stand at −20 °C, we were able to grow large single crystals of the sparingly soluble dark brown compound, which was confirmed by X-ray crystallography to be the μ-oxo complex $(Me_2C_6H_3)_3Ir{-}O{-}Ir(C_6H_3Me_2)_3$ (Figure 1). The compound crystallizes in the cubic space group $Pa\bar{3}$ (Table 1), with the complex sitting on a crystallographic threefold axis with the bridging oxygen atom on the inversion center. The molecule therefore has crystallographically required S_6 symmetry. In particular, the μ-oxo bridge is strictly linear, and the three-bladed propellers formed by the aryl groups surrounding each iridium have opposing chirality. A linear μ-oxo bridge was also seen in the isoelectronic neopentylrhodium(IV) complex $(Me_3CCH_2)_3Rh{-}O{-}Rh(CH_2CMe_3)_3$.[25] The geometry of the triaryliridium fragment (Ir—C distance of 2.007(2) Å, C—Ir—C angles of 106.43(5)°) is remarkably similar to what is found in both trimesityliridium(III) (2.00 Å av, 107.5° av)[8] and oxotrimesityliridium(V) (2.015 Å av, 108.9° av)[7] (Table 2).

Table 2. Selected Bond Lengths (Å) and Angles (deg) for $(2,6\text{-}Me_2C_6H_3)_3Ir{-}O{-}Ir(C_6H_3\text{-}2,6\text{-}Me_2)_3{\cdot}CD_2Cl_2$, Compared with Corresponding Parameters in $(mes)_3Ir$[a] and $(mes)_3Ir{=}O$[b]

	$(mes)_3Ir$[a]	$Ar_3Ir{-}O{-}IrAr_3$ Ar = 2,6-$Me_2C_6H_3$	$(mes)_3Ir{=}O$[b]
Ir—C, Å	2.00[4] av	2.007(2)	2.015[19] av
	2.01	*2.04*	*2.05*
Ir—O, Å	n/a	1.9142(1)	1.725(9)
		1.92	*1.74*
C—Ir—C, deg	107.5[17] av	106.43(5)	109[6] av
	106.5	*94.6*	*101.2*
C—Ir—O, deg	n/a	112.36(4)	110[6] av
		121.5	*116.7*
Ir—O—Ir, deg	n/a	180.0	n/a
		170.5	

[a] Reference 8. [b] Reference 7. [c] Numbers in parentheses represent estimated standard deviations in the last digits of single crystallographically measured values; values in brackets represent standard deviations in the average of the three independent measurements in the molecule. Values in italics are the results of DFT calculations on the $(CH_3)_3Ir$ analogues of the triaryliridium complexes.

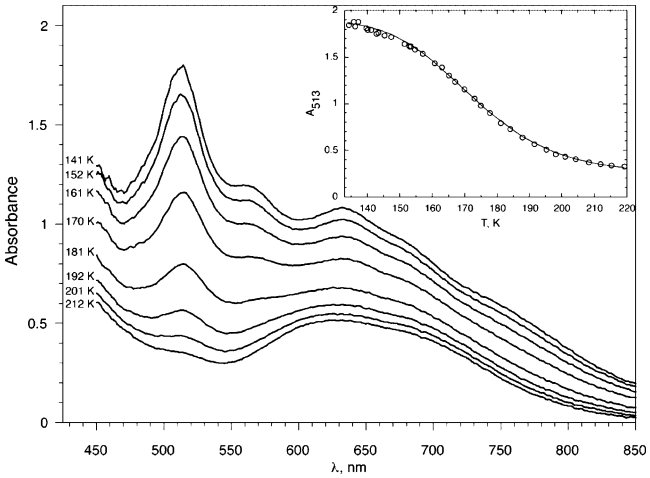

Figure 2. Optical spectra of a mixture of $(mes)_3Ir$ and $(mes)_3Ir{=}O$ as a function of temperature (20:1 $CHFCl_2/CD_2Cl_2$, total [Ir] = 1.2×10^{-3} M, 0.2 mm path length). Temperatures are indicated on the left. Inset: Absorbance at 513 nm as a function of temperature. The solid line is the fit calculated on the basis of the thermodynamic parameters for conproportionation given in the text.

The change of color from green to brown on cooling solutions of partially reduced $(mes)_3Ir{=}O$ can be analyzed quantitatively by low-temperature optical spectroscopy. As the temperature of solutions of $(mes)_3Ir{=}O/(mes)_3Ir$ mixtures are lowered below about −60 °C, the absorbance of the solution increases at all wavelengths longer than 450 nm (Figure 2). The μ-oxo complex has a particularly strong absorption at 513 nm (ϵ = 25 400 M^{-1} cm^{-1}) and also shows two other intense peaks at 560 and 632 nm, as well as shoulders at longer wavelengths (675, 736 nm). Similar behavior is observed in CH_2Cl_2 or in mixtures of

(25) Hay-Motherwell, R. S.; Wilkinson, G.; Hussain-Bates, B.; Hursthouse, M. B. *Polyhedron* **1990**, *9*, 2071−2080.

dichloromethane and $CHFCl_2$ (Freon-21), although the Freon mixture is preferred for quantitative studies because it remains fluid at the extremely low temperatures (~140 K) needed to shift the equilibrium strongly toward the μ-oxo complex at the submillimolar concentrations required for optical spectroscopy. The rise in absorbance at 513 nm as the temperature is lowered is directly proportional to the concentration of the limiting reagent of eq 4, consistent with a 1:1 stoichiometry of $(mes)_3Ir{=}O$ and $(mes)_3Ir$. Runs conducted at different iridium concentrations give consistent values for the K_{eq} of eq 4, and analysis of the temperature-dependence of the absorbance from 135 to 220 K (inset, Figure 2) allows the determination of the thermodynamic parameters $\Delta H°_4 = -5.14 \pm 0.13$ kcal/mol and $\Delta S°_4 = -15.2 \pm 0.7$ cal/mol·K.

$$(mes)_3Ir{=}O + Ir(mes)_3 \leftrightarrows (mes)_3Ir{-}O{-}Ir(mes)_3 \quad (4)$$

Kinetics of Dissociation of $(mes)_3Ir{-}O{-}Ir(mes)_3$. ^1H NMR spectra of equilibrium mixtures of $(mes)_3Ir{=}O$, $(mes)_3Ir{-}O{-}Ir(mes)_3$, and $(mes)_3Ir$ recorded above about −80 °C show only a single set of mesityl resonances due to the rapid exchange of mesityl environments among the three species. Both aromatic hydrogens appear as a single resonance, as do both *ortho*-methyl groups. However, these resonances do show some broadening as the temperature is lowered to −80 °C, due to hindered Ir—C bond rotation in the three species. The iridium(III) complex was previously reported to exhibit a sizable barrier to Ir—C bond rotation ($\Delta G^‡ = 13.0$ kcal/mol, extrapolated to 163 K)[6,8] and shows sharp, separate signals for the aromatic and *o*-methyl peaks even at −20 °C. In contrast, the oxo complex $(mes)_3Ir{=}O$ shows a much faster Ir—C bond rotation. Even at −110 °C, the aromatic resonance, though slightly broadened, is still coalesced. However, at this low temperature the *o*-CH_3 resonances of $(mes)_3Ir{=}O$ have decoalesced sufficiently to determine their chemical shifts (Figure S1), and this allows line shape analysis over the range −110 to −80 °C, giving thermodynamic parameters for Ir—C bond rotation in $(mes)_3Ir{=}O$ (Figure S2) of $\Delta H^‡ = 5.73 \pm 0.04$ kcal/mol, $\Delta S^‡ = -9.80 \pm 0.24$ cal/mol·K, and $\Delta G^‡$ (163 K) = 7.33 kcal/mol.

At temperatures above about −80 °C, the *para*-methyl resonance, which is insensitive to bond rotation but does change chemical shift with iridium oxidation state, remains a single sharp resonance in Ir(V)/Ir(IV)/Ir(III) mixtures. At temperatures below −80 °C, this resonance broadens and decoalesces as the rate of intermolecular exchange slows (Figure 3). The aromatic and *ortho*-methyl resonances likewise broaden and separate, although the detailed lineshapes of these resonances are complicated by the effects of intramolecular exchange due to Ir—C bond rotation. The low-temperature limiting spectra show only the μ-oxo complex $(mes)_3Ir{-}O{-}Ir(mes)_3$ and one of the monomeric iridium species, $(mes)_3Ir$ or $(mes)_3Ir{=}O$, depending on whether more or less than half of the oxygen has been removed. At these concentrations and this low temperature, the position of the equilibrium strongly favors conproportionation. Note that the aromatic and *ortho*-methyl resonances of $(mes)_3Ir{-}O{-}Ir(mes)_3$ are well-separated, but still slightly broadened, at −110°, indicating that the barrier to Ir—C bond rotation in the μ-oxodiiridium(IV) complex ($k_{rot} = 40\ s^{-1}$, $\Delta G^‡ = 8.1$ kcal/mol at 163 K) is intermediate between that of Ir(III) and Ir(V). This correlation of rotation barrier with the electronic unsaturation at iridium, rather than with steric hindrance, substantiates

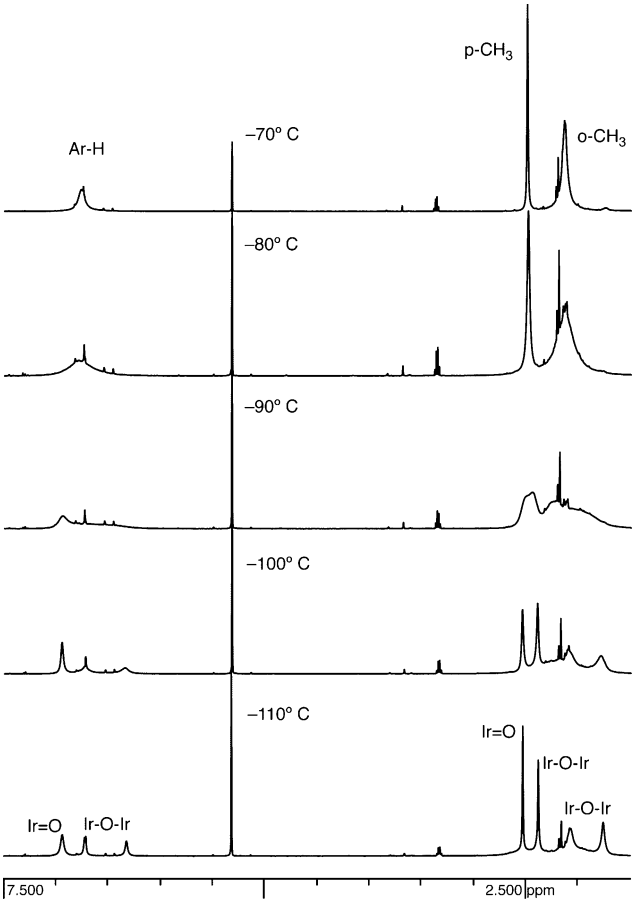

Figure 3. Variable-temperature 500-MHz ^1H NMR spectra of a $(mes)_3Ir{-}O{-}Ir(mes)_3/(mes)_3Ir{=}O$ mixture in CD_2Cl_2 over the range −70 to −110 °C. The *ortho*-CH_3 groups of $(mes)_3Ir{=}O$ at −110 °C appear as a broad, partially decoalesced peak from 1.8−2.6 ppm (see Figure S1).

our earlier contention that agostic interactions between iridium and the *ortho*-methyl groups are significant in $(mes)_3Ir$.[6]

The line shape of the *para*-methyl peaks can be analyzed in the temperature range −80 to −102.5 °C to determine the rate of dissociation of $(mes)_3Ir{-}O{-}Ir(mes)_3$ to give $(mes)_3Ir{=}O$ and $(mes)_3Ir$ (Figure 3; note that at these concentrations and temperatures conproportionation is highly favorable, so only one of $(mes)_3Ir{=}O$ or $(mes)_3Ir$ will be present in appreciable concentration, depending on whether the average oxidation state is greater than or less than +4). The rate constants k_{diss} obtained by line shape analysis are independent within experimental error of whether the observed exchange is between Ir(IV) and Ir(V) or between Ir(IV) and Ir(III), and are independent of whether the mixture of oxidation states is generated by the slow spontaneous reduction of $(mes)_3Ir{=}O$ in CD_2Cl_2 or by deliberate addition of substoichiometric PPh_3 (a process that has been shown to generate $(mes)_3Ir$ cleanly[6]), substantiating a mechanism involving simple, unassisted dissociation of the μ-oxo dimer without participation of other species such as $OPPh_3$ (if present). An Eyring plot (Figure S3) gives the activation parameters for the dissociation of the μ-oxo complex as $\Delta H^‡_{diss} = 10.04 \pm 0.14$ kcal/mol, $\Delta S^‡_{diss} = +8.6 \pm 0.8$ cal/mol·K. Combining these activation parameters with the thermodynamic parameters for the net reaction of eq 4 allows one to compute activation parameters for the forward direction of eq 4 (neglecting the difference between the 95% $CHFCl_2$/5% CD_2Cl_2 used for

equilibrium measurements and the CD_2Cl_2 used for kinetics): $\Delta H^{\ddagger}_{IrIr} = 4.90 \pm 0.19$ kcal/mol, $\Delta S^{\ddagger}_{IrIr} = -6.6 \pm 1.1$ cal/mol·K, $\Delta G^{\ddagger}_{IrIr}$ (293 K) $= 6.83 \pm 0.36$ kcal/mol. Using these data to extrapolate the rate constant for bimolecular degenerate atom transfer to 293 K, where conproportionation is the rate-determining step in complete oxygen atom transfer, gives $k_{IrIr} = 5 \times 10^7$ M^{-1} s^{-1}.

Oxygen Atom Cross-Exchange Reactivity of $(ArN)_3Os{=}O.$ In order to better understand the features that make $(mes)_3Ir{=}O$ so kinetically reactive toward oxygen atom self-exchange, we sought a system that might share a number of the unusual features of the $(mes)_3Ir{=}O/(mes)_3Ir$ redox couple. The tris(imido) osmium complexes $(ArN)_3Os{=}O$ and $(ArN)_3Os$ (Ar = 2,6-diisopropylphenyl), described by Schrock and co-workers,[9] appeared to be an ideal comparison: Both pairs of complexes involve low-coordinate, late transition metal oxo complexes, and in both instances the reduced species are stable as three-coordinate monomers which do not readily bind additional ligands.

The osmium oxo complex $(ArN)_3Os{=}O$ also appears to be similar to $(mes)_3Ir{=}O$ in its reactivity toward main group oxygen atom acceptors. The osmium oxo complex undergoes clean reduction by triphenylphosphine to form $OPPh_3$ and $(ArN)_3Os$ in a reaction that is first-order in both reagents (eq 5). The activation parameters for this reduction (289−331 K, 1,2-dichlorobenzene, Figure S4), $\Delta H^{\ddagger} = 7.7 \pm 0.3$ kcal/mol, and $\Delta S^{\ddagger} = -30.3 \pm 1.1$ cal/mol·K, show the large negative activation entropy typical of bimolecular oxygen atom transfer reactions.[4b] At room temperature, the rate constant k_{OsP} is 1.30(7) M^{-1} s^{-1} (25 °C, CH_2Cl_2), only three times smaller than the corresponding rate constant for iridium[6] ($k_{IrP} = 3.95$ M^{-1} s^{-1}).

$$(ArN)_3Os{=}O + PPh_3 \xrightarrow{k_{OsP}} (ArN)_3Os + OPPh_3 \qquad (5)$$

Even more remarkably, the osmium and iridium complexes have nearly equivalent thermodynamic propensities toward oxygen atom transfer. Within minutes at room temperature, intermetal oxygen atom transfer takes place between $(mes)_3Ir{=}O$ and $(ArN)_3Os$ to give an equilibrium mixture of both oxo complexes and both reduced species (eq 6), with $K_{IrOs} = 0.6$ in CD_2Cl_2 at 20 °C. The position of equilibrium is only slightly temperature-dependent, with a van't Hoff plot between 243 and 288 K giving $\Delta H^{\circ}_{IrOs} = -0.86 \pm 0.03$ kcal/mol and $\Delta S^{\circ}_{IrOs} = -3.89 \pm 0.10$ cal/mol·K (Figure S5). In this temperature range the formation of the iridium(IV) μ-oxo complex is negligble, and there is no evidence by NMR for any interaction between $(ArN)_3Os{=}O$ and $(ArN)_3Os$ at any temperature. Since the reaction shown in eq 6 corresponds to breaking an Ir=O bond and forming an Os=O bond, the small ΔH° indicates that the bond dissociation enthalpies of the two bonds are nearly equal, with the Os=O bond having the greater BDE by 0.86 kcal/mol.

$$(mes)_3Ir{=}O + (ArN)_3Os \leftrightarrows (mes)_3Ir + (ArN)_3Os{=}O \qquad (6)$$

While the rate of cross-exchange (eq 6) is rapid at room temperature, rates can be measured between −70 and −30 °C by observing the growth of the resonances of $(ArN)_3Os{=}O$ as well as the changes in the positions of the mesityl resonances, which shift upfield as $(mes)_3Ir{=}O$ is deoxygenated to an equilibrium mixture of $(mes)_3Ir{-}O{-}Ir(mes)_3$ and $(mes)_3Ir$. The measured initial rates of reaction are proportional to both [Ir] and [Os], and the variation of the observed second-order rate constants k_{IrOs} with temperature (Figure S6) allows one to calculate activation parameters for the cross-exchange reaction of eq 6 (in the forward direction): $\Delta H^{\ddagger}_{IrOs} = 11.3 \pm 0.5$ kcal/mol and $\Delta S^{\ddagger}_{IrOs} = -15.3 \pm 2.4$ cal/mol·K.

Scheme 1. Preparation of Labeled $Os(NAr_D)_3$

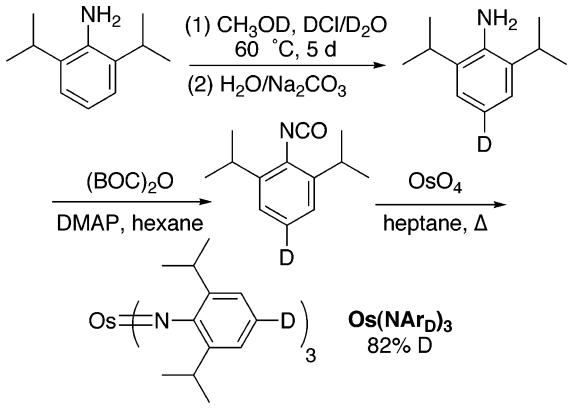

Oxygen Atom Self-Exchange of $(ArN)_3Os/(ArN)_3Os{=}O.$ Degenerate intermetal oxygen atom transfer between $(ArN)_3Os$ and $(ArN)_3Os{=}O$ is slow, with mixtures of the two osmium complexes showing sharp, separate, unperturbed NMR resonances for both complexes even at +100 °C in toluene-d_8. In order to measure exchange between the two species on the chemical time scale, we prepared the tris(imido)osmium(VI) complex labeled in the para position with deuterium, $(Ar_DN)_3Os$ (Scheme 1).

Upon mixing $Os(NAr_D)_3$ with unlabeled $(ArN)_3Os{=}O$, growth of the para resonance of the osmium(VI) complex in the ^1H NMR is exceedingly slow, requiring weeks to achieve equilibrium at room temperature. Kinetics of isotope exchange were measured in benzene, since $(ArN)_3Os{=}O$ decomposes in dichloromethane at a significant rate on the extremely slow time scale of the reaction. The reactions exhibited a moderate degree of autocatalysis, with the apparent rate constants increasing after the first half-life or so. The origin of the autocatalysis is unknown, but it is not due to production of trace amounts of free aniline, since spiking the mixture with 2,6-diisopropylaniline does not accelerate exchange. However, reaction rates measured in the first half-life or so are reproducible, and redistribution of the deuterium conforms to the pseudo-first-order decay expected for exchange kinetics, regardless of the rate law.[18] The fact that the observed rate constant is proportional to the total osmium concentration (Figure S7) indicates that the reaction is second-order, and from seven runs at 20 °C, the average rate constant k_{OsOs} is $(1.8 \pm 0.2) \times 10^{-5}$ M^{-1} s^{-1}.

The NMR analysis of isotope exchange measures the rate at which the imido groups exchange environments between osmium(VI) and osmium(VIII) but cannot distinguish between oxygen atom transfer between $(ArN)_3Os{=}O$ and $(ArN)_3Os$ or direct imido group exchange between osmium centers. These two processes can be distinguished by mass spectrometry, since oxygen atom exchange retains the integrity of a tris(imido)osmium unit, while imido exchange severs the correlation any individual imido group once had with its fellows in the $Os(NAr)_3$ fragment, and must therefore result in a completely

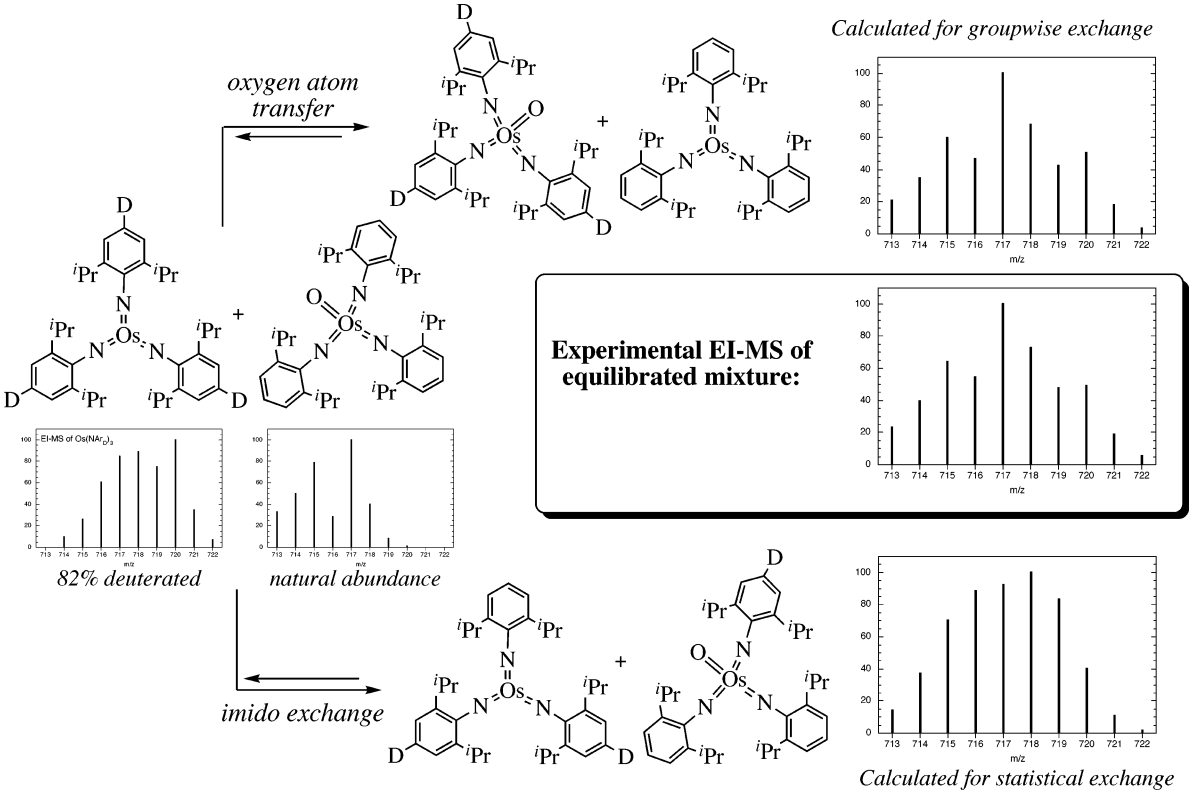

Figure 4. Mass spectrometric analysis of the isotopic composition of $Os(NAr)_3$ after equilibration of deuterium-enriched $Os(NAr_D)_3$ and unlabeled O═$Os(NAr)_3$ (middle right). Isotope patterns of the parent ions of the 82% deuterated $Os(NAr_D)_3$ and natural-abundance $Os(NAr)_3$ are shown on the lower left. Isotope patterns calculated for the equilibrium mixture given the measured overall composition and assuming either an oxygen atom transfer mechanism (upper right) or an individual imido group transfer mechanism (lower right) are shown for comparison with the observed pattern.

statistical distribution of imido groups (Figure 4). The experimental data are highly nonstatistical and clearly exclude any significant amount of exchange of individual imido groups. Agreement with the groupwise exchange model is excellent, consistent with assignment of the observed exchange to an oxygen atom transfer process.

Application of Intermetal Oxygen Atom Transfer to Cocatalyzed Air Oxidations. Oxotrimesityliridium(V) is inert to all common organic functional groups, reacting only with very easily oxidized substrates such as phosphines and arsines.[6] Thus, despite the fact that $(mes)_3Ir$ activates O_2 readily to form the oxo compound, its use as a catalyst in air oxidations is limited. However, the great kinetic facility of $(mes)_3Ir$═O in inter*metal* oxygen atom transfer reactions suggests that it could be used in tandem with other oxometal reagents to allow greater scope for catalyzed air oxidations.

The goal of cocatalyzed air oxidation has been achieved using quinuclidine-ligated OsO_4 as a cocatalyst with $(mes)_3Ir$═O in two different reactions. First, this reagent combination mediates the well-known dihydroxylation of olefins[26] using air and water as stoichiometric reagents. Air has been used as the terminal oxidant in dihydroxylations under organic/basic aqueous biphasic conditions,[27] but no turnover is seen in organic solvents. However, in the presence of catalytic $(mes)_3Ir$═O, a variety of monosubstituted alkenes react with air and water in the presence of catalytic $(C_7H_{13}N)OsO_4$ and $(mes)_3Ir$═O to give 1,2-diols (eq 7). Diols are the sole product of oxidation of aliphatic alkenes, and functional group compatibility is good. Arylalkenes give lower yields of diols (75% for styrene to 1,2-phenylethanediol), presumably because of overoxidation of the benzylic alcohol in the product (see below).

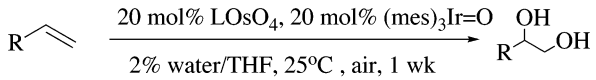

(7)

R = Ph, ^{n}C$_6$H$_{13}$, AcO(CH$_2$)$_3$, EtOCH$_2$, PhCH$_2$

Unfortunately, the rate of dihydroxylation is very low (5 turnovers/week), and the reaction is limited to monosubstituted alkenes. More highly substituted alkenes react readily with osmium to form glycolates, but these glycolates do not react with iridium at appreciable rates. Monitoring the reaction over time (Figure S8) indicates that the reaction slows down considerably as it progresses. This is not due to catalyst degradation, as the $(mes)_3Ir$═O and the osmium glycolate concentrations, as monitored by ^{1}H NMR, are unchanged over the course of the reaction. Instead the slowdown is accounted for, quantitatively, by inhibition by the diol product.

1-Octene can be dihydroxylated enantioselectively with catalytic OsO_4 and $(mes)_3Ir$═O using $(DHQD)_2PHAL$.[28] While the reaction occurs with a modest 45 (±2)% ee, this is identical

(26) Schröder, M. *Chem. Rev.* **1980**, *80*, 187−213.
(27) (a) Döbler, C.; Mehltretter, G.; Beller, M. *Angew. Chem., Int. Ed.* **1999**, *38*, 3026−3028. (b) Döbler, C.; Mehltretter, G. M.; Sundermeier, U.; Beller, M. *J. Am. Chem. Soc.* **2000**, *122*, 10289−10297. (c) Döbler, C.; Mehltretter, G. M.; Sundermeier, U.; Beller, M. *J. Organomet. Chem.* **2001**, *621*, 70−76.
(28) (a) Kolb, H. C.; Van, Nieuwenhze, M. S.; Sharpless, K. B. *Chem. Rev.* **1994**, *94*, 2483−2547. (b) Johnson, R. A.; Sharpless, B. K. In *Catalytic Asymmetric Synthesis*, 2nd ed.; Ojima, I., Ed.; Wiley-VCH: New York, 2000; Chapter 6.

to that shown by stoichiometric OsO_4/$(DHQD)_2PHAL$ under the same conditions. The lower enantioselectivity than achieved under the optimized Sharpless conditions is attributed to the solvent (THF compared to $^tBuOH/H_2O$). The equivalence of the selectivity under stoichiometric and catalytic conditions demonstrates that the $(mes)_3Ir{=}O$ does not participate directly in the osmylation of the olefin and acts solely as a reoxidant for the osmium.

Oxotrimesityliridium(V) can also cocatalyze the room-temperature air oxidation of benzylic and allylic alcohols to the corresponding aldehydes and ketones. Here the cooxidant is $(C_7H_{13}N)OsO_4$ prereduced with a sacrificial alkene such as vinyl acetate or allyl ethyl ether, as was previously described using copper salts as the oxygen-activating component.[29] Because alcohol oxidation is not inhibited by the product carbonyl compounds in the way that alkene oxidation is inhibited by the product diols, much higher turnover numbers can be achieved. Thus, complete oxidation of a variety of allyl and benzyl alcohols at atmospheric pressure is routinely achieved in 3 days in THF using 2 mol % of alkene-activated $(C_7H_{13}N)OsO_4$ and 1 mol % of $O{=}Ir(mes)_3$. The scope (primary and secondary benzylic and allylic alcohols, toleration of other oxidizable functional groups such as alkenes), selectivity (no overoxidation to the carboxylic acid, no oxidation of aliphatic alcohols), and limitations (1,2- and 1,3-diols prevent reaction) are the same as those discussed previously for the osmium/copper-catalyzed oxidation.[29] Rates are generally somewhat slower than those for the copper-catalyzed process, which requires only about 18 h to go to completion using similar catalyst loadings.

Discussion

Factors Governing Rates of Intermetal Oxygen Atom Transfer. Oxygen atom transfer between transition metal centers is generally accepted to proceed via a μ-oxo intermediate (cf. eq 1). In many cases conproportionation is favored and μ-oxo complexes are the final observed products.[30] Quantitative studies of the rates of intermetal oxygen atom transfer reactions are surprisingly rare. One well-characterized example is the molybdenum(VI)/molybdenum(IV) redox couple $(dtc)_2MoO_2$/$(dtc)_2MoO$ (dtc = *N*,*N*-diethyldithiocarbamate), where oxygen atom transfer proceeds through an observable molybdenum(V) intermediate, $(dtc)_2Mo(O){-}O{-}Mo(O)(dtc)_2$ (eq 8). In fact, con-

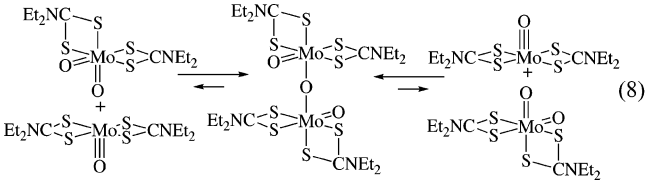

(8)

proportionation in this system is thermodynamically favored (K_{eq} = 500 M^{-1} at 298 K) and proceeds at a moderate rate (k_{MoMo} = 1470 M^{-1} s^{-1}).[31] Woo and co-workers have also examined near-degenerate oxygen/chlorine exchange in porphyrinato chromium[32] and titanium complexes[33] (TTP)M=O/(OEP)MCl. While these are not classical oxygen atom transfer reactions, since they involve only net one-electron transfer, they are related in that they involve electron transfer through an oxygen bridge. Rates range from 0.1 M^{-1} s^{-1} (Cr) to 240 M^{-1} s^{-1} (Ti).

Given these moderate rates, the extreme facility of oxygen atom transfer between $(mes)_3Ir{=}O$ and $(mes)_3Ir$, with $k_{IrIr} = 5 \times 10^7$ M^{-1} s^{-1} at 20 °C, is remarkable. Although the dearth of quantitative measurements makes comparison difficult, we know of no other examples where a metal oxo complex and its deoxy form are in rapid exchange by NMR at any temperature; $(mes)_3Ir$ and $(mes)_3Ir{=}O$ are in rapid exchange by NMR even at −80 °C. Even highly exothermic oxygen atom transfer reactions, such as the ~70-kcal/mol downhill[34] oxidation of PPh_3 by $[Ru(bpy)_2(py)(O)]^{2+}$ ($k_{RuP} = 1.75 \times 10^5$ M^{-1} s^{-1}),[4a] proceed at slower rates than this degenerate intermetal atom transfer. While there are examples of electron transfer and one-electron atom transfer reactions[35] between transition metal centers that proceed at comparable (or faster) rates, the only two-electron atom transfer self-exchange reaction that approaches this rate is the degenerate transfer of I^+ between $[Cp_2RuI]^+$ and Cp_2Ru ($k \approx 7 \times 10^5$ M^{-1} s^{-1}, 20 °C, CD_3CN),[36] and the rapid rate in this case is contingent on the heavy halogen, with the chlorine analogue undergoing atom transfer at only 16.5 M^{-1} s^{-1}.[37]

One obvious reason for the rapidity of the oxygen atom transfer process compared to other examples in the literature is that intrinsic rates are often obscured by rearrangements of the ancillary ligands that accompany the redox chemistry. The dithiocarbamate ligands in the molybdenum(IV) complex $(dtc)_2MoO$ must rearrange from trans to cis in order to form the molybdenum(V) μ-oxo complex (eq 8), and chloride transfer is required in addition to oxygen transfer in the porphyrinato-chromium or -titanium reactions. Often, the complex in the lower oxidation state binds a ligand which must dissociate to open a site to accommodate the bridging oxygen.

In contrast, the $(mes)_3IrO$/$(mes)_3Ir$ and $(ArN)_3OsO$/$(ArN)_3Os$ redox couples examined here are well-suited to studying oxygen atom transfer free from complications of ligand dissociation or rearrangement. Both compounds exist in the lower oxidation state as stable, three-coordinate monomers. Oxygen atom transfer can take place near thermoneutrality among these complexes (Table 3), not only in the degenerate reactions but also in the cross-exchange reaction ($K_{IrOs} = 0.6$ at 293 K). Even conproportionation of $(mes)_3IrO$ with $(mes)_3Ir$ to form the μ-oxo complex $(mes)_3Ir{-}O{-}Ir(mes)_3$ is not strongly favored at room temperature ($\Delta G° = -0.69$ kcal/mol at 293 K).

Comparison of the iridium and osmium systems demonstrates that ancillary ligand dissociation or rearrangement is not the only factor limiting oxygen atom transfer rates between metals. Despite the thermodynamic and structural similarities between the iridium and osmium systems, atom transfer in the two systems takes place at vastly differing rates. $(ArN)_3Os{=}O$ transfers its oxygen atom to $(ArN)_3Os$ with a rate constant of

(29) Muldoon, J.; Brown, S. N. *Org. Lett.* **2002**, *4*, 1043−1045.
(30) Woo, L. K. *Chem. Rev.* **1993**, *93*, 1125−1136.
(31) Matsuda, T.; Tanaka, K.; Tanaka, T. *Inorg. Chem.* **1979**, *18*, 454−457.
(32) Woo, L. K.; Goll, J. G.; Berreau, L. M.; Weaving, R. *J. Am. Chem. Soc.* **1992**, *114*, 7411−7415.
(33) Hays, J. A.; Day, C. L.; Young, V. G.; Woo, L. K. *Inorg. Chem.* **1996**, *35*, 7601−7607.
(34) Estimated from the phosphorus−oxygen bond strength of 133 kcal/mol (ref 3b) and the electrochemical data in Moyer, B. A.; Meyer, T. J. *Inorg. Chem.* **1981**, *20*, 436−444.
(35) (a) Song, J.-S.; Bullock, R. M.; Creutz, C. *J. Am. Chem. Soc.* **1991**, *113*, 9862−9864. (b) Creutz, C.; Song, J.-S.; Bullock, R. M. *Pure Appl. Chem.* **1995**, *67*, 47−54.
(36) (a) Smith, T. P.; Iverson, D. J.; Droege, M. W.; Kwan, K. S.; Taube, H. *Inorg. Chem.* **1987**, *26*, 2882−2884. (b) Kirchner, K.; Dodgen, H. W.; Wherland, S.; Hunt, J. P. *Inorg. Chem.* **1990**, *29*, 2381−2385.
(37) Shea, T. M.; Deraniyagala, S. P.; Studebaker, D. B.; Westmoreland, T. D. *Inorg. Chem.* **1996**, *35*, 7699−7703.

Table 3. Summary of Experimental and Calculated Thermodynamic and Kinetic Parameters for Oxygen Atom Transfer between R_3Ir/$R_3Ir{=}O$ and $(R'N)_3Os$/$(R'N)_3Os{=}O$[a]

	$R_3Ir{=}O + IrR_3 \rightarrow$ $R_3Ir{-}O{-}IrR_3$	$R_3Ir{=}O + Os(NR')_3 \rightarrow$ $R_3Ir + O{=}Os(NR')_3$	$(R'N)_3Os{=}O + Os(NR')_3 \rightarrow$ $(R'N)_3Os + O{=}Os(NR')_3$
$\Delta H°$ (kcal/mol)	−5.14(13)	−0.86(3)	0
	−17.7	*17.7*	
$\Delta S°$ (cal/mol·K)	−15.2(7)	−3.89(10)	0
	−29.1	*−5.2*	
$\Delta G°$ (kcal/mol, 293 K)	−0.69(24)	0.28(4)	0
	−9.1	*19.4*	
$\Delta H^{‡}$ (kcal/mol)	4.90(19)	11.3(5)	*b*
$\Delta S^{‡}$ (cal/mol·K)	−6.6(11)	−15.3(24)	*b*
$\Delta G^{‡}$ (kcal/mol, 293 K)	6.8(4)	15.8(9)	23.50(6)
k (293 K, M^{-1} s^{-1})	5×10^{7}[c]	1.0×10^{1}[c]	$1.8(2) \times 10^{-5}$

[a] Experimental values are given in roman type for R = mes, R′ = 2,6-$^{i}Pr_2C_6H_3$, with calculated values in italic type for R = R′ = CH_3. All $\Delta G°$ values are at 293 K. [b] Not measured. [c] Extrapolated to 293 K.

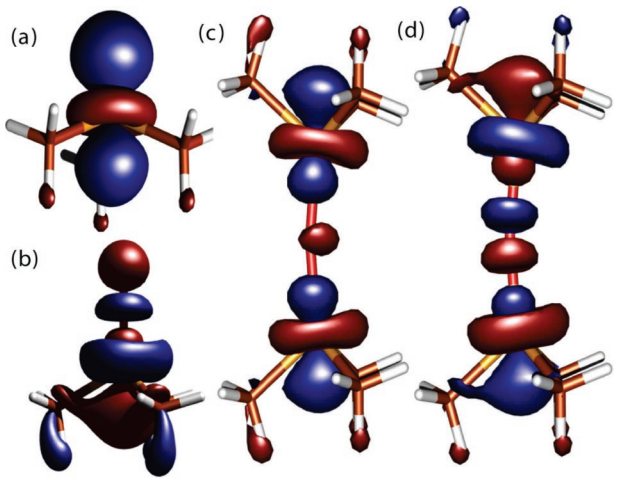

Figure 5. Frontier orbitals of $(CH_3)_3Ir$, $(CH_3)_3Ir{=}O$, and $(CH_3)_3Ir{-}O{-}Ir(CH_3)_3$. (a) $(CH_3)_3Ir$ HOMO, $E = -5.65$ eV. (b) $(CH_3)_3Ir{=}O$ LUMO, $E = -2.61$ eV. (c) $(CH_3)_3Ir{-}O{-}Ir(CH_3)_3$ HOMO, $E = -5.30$ eV. (d) $(CH_3)_3Ir{-}O{-}Ir(CH_3)_3$ LUMO, $E = -2.80$ eV.

only 1.8×10^{-5} M^{-1} s^{-1}, *12 orders of magnitude* slower than the analogous reaction of iridium.

The facility of oxygen transfer between iridium centers can be illuminated by an analysis of the bonding in the iridium-(III), (IV), and (V) complexes. The effective C_{3v} symmetry of the $(mes)_3Ir$ fragment implies that the iridium d orbitals split into two pairs of e symmetry and a lone orbital of a_1 symmetry. In order for d^6 $(mes)_3Ir$ to be diamagnetic, one e set and the a_1 orbital (derived from the Ir d_{z^2}) must be occupied. This is confirmed by DFT calculations (on $(CH_3)_3Ir$), which indicate that the a_1 orbital is the HOMO (Figure 5). Analogous symmetry arguments applied to diamagnetic d^4 $(mes)_3Ir{=}O$ indicate that the a_1 orbital in this case must be empty; DFT calculations indicate that this Ir−O σ^* orbital is the LUMO of the complex. Interaction of the hydrocarbyl ligands with these orbitals is minimal because they lie approximately in the nodal cone of d_{z^2}.

In a linear μ-oxo dimer of approximately D_{3d} symmetry, the two d_{z^2} orbitals will combine to form orbitals of a_{1g} and a_{2u} symmetry. Again, the observed diamagnetism of the dimer, with 10 d electrons, requires that exactly 1 of these 2 orbitals is filled (since all the other d orbitals occur as degenerate pairs). DFT calculations indicate that the former orbital is the HOMO and the latter is the LUMO of the complex, with a sizable energy gap of 2.5 eV between them. The a_{2u} orbital interacts with the oxygen 2p orbital and is strongly Ir−O σ^* in character. The a_{1g} combination, in contrast, can interact only with the 2s orbital on oxygen, and this orbital is much lower-lying than the 2p.[38] The energy match with iridium is correspondingly poor, so the a_{1g} orbital is only weakly antibonding, and remains low in energy.

All of these orbitals lie along the *z*-axis. Thus, as $(mes)_3Ir$ approaches $O{=}Ir(mes)_3$, the nonbonding pair of electrons in its a_1 orbital can interact with the a_1 LUMO of the oxo complex, ending up in the low-lying a_{1g} orbital. Productive dissociation follows the microscopic reverse pathway, with the roles of the iridium atoms interchanged. Only a modest barrier is expected to this allowed reaction, consistent with the observed high rates. Calculations in the gas phase do not find any barrier to conproportionation and overestimate the stability of the μ-oxo complex (Table 3). Solvation might partially account for the differences between the calculations and observations, as the smaller accessible surface of the dimer with respect to the two monomers would make it (and presumably the transition state) less enthalpically (though more entropically) favorable in solution than in the gas phase. The smaller size of the methyl groups used in the calculation is also expected to exaggerate the calculated stability of the μ-oxo complex compared to the mesityl complex. For these reasons, and because of the inherent difficulties in calculations involving third-row transition metals, it is not expected that the computed thermodynamic values would be quantitatively accurate. Nevertheless, the agreement between the experimental and computed geometries (Table 2) indicates that the results from electronic structure calculations can be used in the qualitative arguments outlined above.

Note that the bonding here differs significantly from that in the tetrahedral monooxo complexes $(silox)_3M{=}O$ (M = Nb, Ta), whose stereoelectronic requirements for oxygen atom transfer have been examined by Wolczanski and co-workers.[39] These early metal oxo complexes are d^0, so their LUMOs are of *E* symmetry, which requires a bent approach to allow oxygen atom transfer. This was experimentally demonstrated in the microscopic reverse direction, in that bulky $^{t}Bu_3PO$, which is

(38) For O, $\epsilon_p - \epsilon_s = 16.5$ eV: Allen, L. C. *J. Am. Chem. Soc.* **1989**, *111*, 9003−9014.

(39) (a) Veige, A. S.; Slaughter, L. M.; Wolczanski, P. T.; Matsunaga, N.; Decker, S. A.; Cundari, T. R. *J. Am. Chem. Soc.* **2001**, *123*, 6419−6420. (b) Veige, A. S.; Slaughter, L. M.; Lobkovsky, E. B.; Wolczanski, P. T.; Matsunaga, N.; Decker, S. A.; Cundari, T. R. *Inorg. Chem.* **2003**, *42*, 6204−6224.

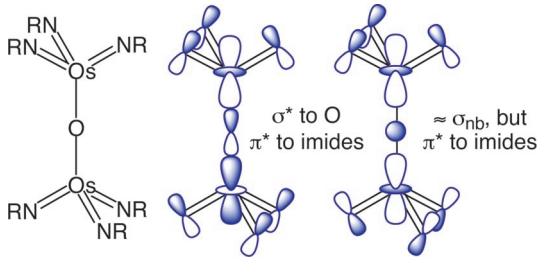

Figure 6. Qualitative orbital interactions in $(RN)_3Os-O-Os(NR)_3$.

sterically inhibited from attaining a bent geometry, is not deoxygenated, while Me_3PO is deoxygenated readily. But in d^4 $(mes)_3Ir{=}O$ the lowest e level is filled, and the symmetry-induced barrier to a linear approach is lifted because of the a_1 symmetry of both the $(mes)_3Ir{=}O$ LUMO and $(mes)_3Ir$ HOMO. The bonding situation in the μ-oxo complex $(mes)_3Ir-O-Ir(mes)_3$ also differs from that of the phosphine oxide complex $(Ph_3PO)Ir(mes)_3$ that is the presumed intermediate in the oxidation of Ph_3P by $O{=}Ir(mes)_3$. In the phosphine oxide complex, the electronic differences between iridium and phosphorus favor localization of the HOMO on iridium rather than phosphorus (in contrast to its delocalization over both iridiums in $(mes)_3Ir-O-Ir(mes)_3$). This filled d_{z^2} orbital would interact unfavorably with the filled orbitals on the oxygen, and in fact the donor complex $(Ph_3P)Ir(mes)_3$ is observed to have a sawhorse geometry, with a substantial barrier to phosphine binding on the threefold axis. This destabilization of the pseudo-tetrahedral geometry of $(Ph_3PO)Ir(mes)_3$ as initially formed by atom transfer has been suggested as one factor contributing to the modest rate of oxidation of PPh_3 by $(mes)_3Ir{=}O$.[6] Oxidation of $(mes)_3Ir$, in contrast, can form the stable linear μ-oxo complex directly.

While $Os(NAr)_3$ is a three-coordinate, late-metal complex like $(mes)_3Ir$, the osmium complex is planar rather than pyramidal.[9] When the $Os(NAr)_3$ fragment pyramidalizes to accept the oxygen atom, the d_{z^2} orbital overlaps with the a_1 combination of nitrogen p orbitals (Figure 6). In fact, *all* the d orbitals are π-antibonding with respect to a pyramidal $M(NR)_3$ fragment.[40] Since a μ-oxo complex of the form $(ArN)_3Os-O-Os(NAr)_3$ must accommodate a pair of d electrons somewhere, this pair of electrons must be π^* in character and the μ-oxo complex is expected to be a high-energy, effectively 20-electron intermediate. This is consistent with the large barrier to degenerate oxygen atom transfer observed in the osmium system. Computationally, all attempts to find a μ-oxo complex $(MeN)_3Os-O-Os(NMe)_3$ as a stable minimum or even a first-order saddle point failed; a scan of the Os−O distance from 3 Å to 2.35 Å with all other coordinates fully optimized leads to a monotonic rise in energy of 10 kcal/mol (Figure S9).

Another way of thinking about these electronic influences on the rate of oxygen atom transfer is to consider them as an inner-sphere reorganization energy. Barriers to single electron transfer in the Marcus framework are principally ascribed to the effects of driving force and reorganization energy λ. The reorganization energy can be further partitioned into an outer-sphere term, λ_o, involving rearrangement of solvent and counterions, and an inner-sphere term, λ_i, which encompasses the changes in bond lengths and angles upon electron transfer. The effect of the λ_i term on electron-transfer rates has been extensively explored.[41]

Viewed from this perspective, the $(mes)_3Ir$ fragment supports exceptionally rapid oxygen atom transfer because it has an exceptionally small inner-sphere reorganization energy. Indeed, crystallographic results on all three oxidation states reveal a $(mes)_3Ir$ fragment whose Ir—C bond lengths and angles are identical within experimental error (Table 2). The only significant bonding change on oxygen transfer takes place along the Ir—O—Ir axis (as it must in order to achieve atom transfer). In contrast, the reduced osmium complex, $Os(NAr)_3$, is planar, while that fragment is pyramidal in $O{=}Os(NAr)_3$. Because of the $d\pi-p\pi$ repulsions on pyramidalization, this bonding change is expected to be energetically costly, and thus $Os(NAr)_3$ is expected to have a substantial inner-sphere reorganization energy and correspondingly slow rates of oxygen atom transfer.

If the bonding changes on atom transfer can be considered analogous to inner-sphere reorganization energy in electron-transfer reactions, then the analogy between the present study and explorations of the Marcus cross-relation is evident. This is the first example where self-exchange and cross-exchange kinetics of oxygen atom transfer have been measured in a system where the thermodynamics of cross-exchange are known. The cross relation has been applied to other one-electron inner-sphere reactions, such as hydrogen atom transfer,[42] as well as to proton transfer,[43] but this appears to be the first example of any multielectron atom transfer reaction to have been examined in this way. For example, while rates have been measured for the two-electron pseudo-self-exchange reactions between nitridometal and chlorometal porphyrins (both Mn(V)/Mn(III)[44] and Cr(V)/Cr(III)[45]) and the corresponding Mn/Cr cross-exchange,[46] the cross-reactions are irreversible and the driving force is unknown. A similar situation is found in the two-electron halogen transfer reactions between Cp_2RuX^+ and Cp_2Os.[36a,37]

The Marcus cross-relation, if applied to the iridium−osmium oxygen atom transfer reaction studied here, predicts that $\Delta G^{\ddagger}_{IrOs} \approx {}^1/_2(\Delta G^{\ddagger}_{IrIr} + \Delta G^{\ddagger}_{OsOs} + \Delta G^{\circ}_{IrOs})$.[47] The activation barrier for cross-exchange calculated in this way is 15.3 ± 0.4 kcal/mol, in excellent agreement with the observed barrier of 15.8 ± 0.9 kcal/mol. While it is far too early to decide whether the Marcus-style analysis of oxygen atom transfer will be generally applicable, its success in this case is part of a growing number of studies that suggest that many of the same principles that govern outer-sphere electron transfer are useful in understanding the rates of atom transfer. In particular, effects of inner-sphere reorganization, whose importance in atom transfer is dramatically illustrated by the system described here, have been applied to explain rates of hydrogen atom transfer,[42] and proton-transfer reactions can in many cases be rationalized by inner-sphere reorganization energy, as in cases where slow proton transfers

(40) Morrison, D. L.; Wigley, D. E. *Inorg. Chem.* **1995**, *34*, 2610−2616.
(41) Stanbury, D. M. *Adv. Chem. Ser.* **1997**, *253*, 165−182.
(42) Roth, J. P.; Yoder, J. C.; Won, T.-J.; Mayer, J. M. *Science* **2001**, *294*, 2524−2526.
(43) Kristjánsdóttir, S. S.; Norton, J. R. *J. Am. Chem. Soc.* **1991**, *113*, 4366−4367.
(44) Woo, L. K.; Goll, J. G.; Czapla, D. J.; Hays, J. A. *J. Am. Chem. Soc.* **1991**, *113*, 8478−8484.
(45) Neely, F. L.; Bottomley, L. A. *Inorg. Chem.* **1997**, *36*, 5432−5434.
(46) Bottomley, L. A.; Neely, F. L. *Inorg. Chem.* **1997**, *36*, 5435−5439.
(47) This neglects the quadratic term $(\Delta G^{\circ}_{IrOs})^2/8(\Delta G^{\ddagger}_{IrIr} + \Delta G^{\ddagger}_{OsOs})$, which is justifiable given the low driving force for the cross-reaction (it amounts to only 3×10^{-4} kcal/mol).

from carbon[48] or from metal hydrides[49] have been attributed to the need to change the geometry and bonding at the center bound to the proton. One is accustomed to thinking of inner-sphere reactions in terms of the electronic details of how bonds can be made and broken. The electronic contrast between the iridium system, where transfer of the oxygen atom in a linear fashion is orbitally allowed, and the osmium system, where it is not, is in line with these expectations. Yet the orbital effects can be viewed as simply another way of expressing inner-sphere reorganization: the $(mes)_3Ir$ fragment is unchanged in the three oxidation states because the bonding changes to oxygen do not affect the metal−carbon bonds, and the electronic difficulties in achieving a μ-oxo complex of osmium are reflected in the energetic cost of pyramidalizing the $Os(NAr)_3$ fragment.

The reorganization energy is certainly not the only factor in atom transfer reactions. Clearly, a key distinction between oxygen atom transfer and both outer-sphere electron transfer and one-electron inner-sphere processes such as hydrogen atom transfer is the presence of an intermediate in oxygen atom transfer reactions. If this intermediate is high in energy, oxygen atom transfer is slow regardless of the degree of inner-sphere reorganization. For example, main group oxygen atom transfer partners such as phosphines and phosphine oxides have structurally similar R_3P fragments, yet direct atom transfer between main group partners is usually vanishingly slow because of the marked instability of a putative μ-oxo intermediate such as $R_3P{-}O{-}PR_3$. Similarly, the fact that $(mes)_3Ir{=}O$ and $(ArN)_3Os{=}O$ both oxidize triphenylphosphine at very similar rates *contradicts* simple predictions based on reorganization energy, which would imply much slower rates of reaction with osmium. The instability of a pseudo-tetrahedral intermediate $(mes)_3Ir(OPPh_3)$ (the phosphine adduct $(mes)_3Ir(PPh_3)$ is over 12 kcal/mol lower in free energy in its saddle-shaped geometry than as a tetrahedron[6]) may contribute to the barrier for phosphine oxidation by iridium in this case.

The thermodynamic instability of the μ-oxo osmium complexes $(ArN)_3Os{-}O{-}MX_3$ is an adequate *qualitative* explanation for the slower rate of intermetal oxygen atom transfer involving osmium. The kinetic effects in intermetal oxygen atom transfer, however, are not negligible: for iridium, essentially thermoneutral formation of the μ-oxo intermediate nevertheless has a 6.8 kcal/mol barrier. The *quantitative* agreement between the observed and calculated cross-reaction rates suggests that not only the thermodynamic effects on the stability of the intermediate but also the kinetic effects in its formation scale linearly on progressing from iridium to osmium.

Use of $(mes)_3Ir{=}O$ as an "Innocent" Dioxygen Activator. Trimesityliridium(III) undergoes extremely rapid oxygen atom transfer with oxotrimesityliridium(V), but this reaction is degenerate and therefore cannot be harnessed to achieve net chemical change. The ability of the $(mes)_3Ir$ fragment to mediate intermetal oxygen atom transfer extends to nondegenerate intermetal atom transfer reactions as well, as demonstrated by the ability of $(mes)_3Ir{=}O$ to oxidize $Os(NAr)_3$ at respectable rates ($k_{IrOs} = 10\ M^{-1}\ s^{-1}$, extrapolated to 293 K).

Combining the ability of $(mes)_3Ir$ to activate O_2 to form $(mes)_3Ir{=}O$[6,7] with the ability of $(mes)_3Ir{=}O$ to transfer its oxygen atom rapidly to other metal centers raises the intriguing possibility of a general scheme for cocatalyzed air oxidation (Scheme 2). Many reagents can oxidize organic substrates but are kinetically unable to be reoxidized by dioxygen. If they were able to accept an oxygen atom from $(mes)_3Ir{=}O$, then the addition of catalytic amounts of oxotrimesityliridium could transform an otherwise stoichiometric organic oxidation to a catalytic one using dioxygen as the stoichiometric oxidant, with potential advantages in cost and environmental impact. Furthermore, since the iridium would interact only with the oxidant and not with the substrate, the selectivity of the oxidation would be that of the stoichiometric reagent and would be unaffected by the iridium.

Scheme 2. Cocatalysis of Aerobic Oxidations by $(mes)_3Ir{=}O$

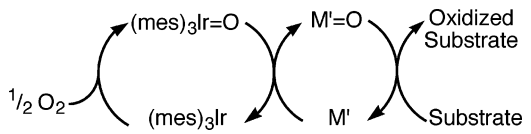

Use of oxotrimesityliridium(V) as a cocatalyst in air oxidations has been demonstrated in two systems: with amine-ligated osmium tetroxide in the dihydroxylation of terminal alkenes,[26] and with osmium(VI) esters in the oxidation of allyl and benzyl alcohols to aldehydes.[29] Both reactions require stoichiometric osmium in the absence of iridium but can use air as the stoichiometric oxidant in the presence of catalytic $(mes)_3Ir{=}O$. The "innocence" of the iridium (the fact that it is not involved in substrate oxidation) is demonstrated in the first reaction by the observation that the enantiomeric excess of 1,2-octanediol using $(DHQD)_2PHAL$ as a chiral ligand is identical in the stoichiometric oxidation and cocatalytic oxidations.

Osmium/iridium-cocatalyzed dihydroxylations are strongly inhibited by the 1,2-diol product (Figure S8), which limits the number of turnovers (~5 per week) and the scope of the reaction (more substituted alkenes, whose diols bind more tightly, do not turn over). The product inhibition supports a mechanism in which reversible loss of diol occurs from the observed osmium(VI) diolate resting state preceding rate-determining oxygen atom transfer from iridium to the osmium complex produced by loss of diol. Assignment of this unobserved osmium species as "OsO_3" (or a ligated form thereof) is plausible, given the stability of isoelectronic $Os(NAr)_3$ and its proven ability to accept an oxygen atom from $(mes)_3Ir{=}O$. Little can be said about the reoxidation step in the alcohol oxidation; it is unknown even whether reoxidation takes place at the Os(IV) or Os(V) oxidation state.

In neither of these particular reactions does use of $(mes)_3Ir{=}O$ represent a practical advance as an oxygen activator, since dioxygen use in both dihydroxylations[50] and alcohol oxidations[51] using osmium is cocatalyzed equally effectively with much cheaper copper salts, and indeed under certain conditions aerobic oxidations of alkenes[27] and alcohols[52] can take place without a cocatalyst (although the selectivity in the latter reaction is different from that observed here). Still, the fact that $(mes)_3Ir{=}O$ can be used as an efficient activator of dioxygen in catalytic

(48) (a) Bernasconi, C. F. *Acc. Chem. Res.* **1992**, *25*, 9−16. (b) Costentin, C.; Savéant, J.-M. *J. Am. Chem. Soc.* **2004**, *126*, 14787−14795.
(49) (a) Kramarz, K. W.; Norton, J. R. *Prog. Inorg. Chem.* **1994**, *42*, 1−65. (b) Jordan, R. F.; Norton, J. R. *J. Am. Chem. Soc.* **1982**, *104*, 1255−1263.
(50) (a) Michaelson, R. C.; Austin, R. G. U.S. Patent 4,390,739 (June 28, 1983). (b) Austin, R. G.; Michaelson, R. C.; Myers, R. S. U.S. Patent 4,824,969 (April 25, 1989).
(51) Coleman, K. S.; Coppe, M.; Thomas, C.; Osborn, J. A. *Tetrahedron Lett.* **1999**, *40*, 3723−3726.
(52) Döbler, C.; Mehltretter, G. M.; Sundermeier, U.; Eckert, M.; Militzer, H.-C.; Beller, M. *Tetrahedron Lett.* **2001**, *42*, 8447−8449.

reactions has potentially important consequences. First, the well-defined nature of the $(mes)_3Ir{=}O/(mes)_3Ir$ redox couple and its inertness to most reactions other than intermetal oxygen atom transfer may make it a suitable cooxidant in delicate systems where copper salts would be unsuitable. For example, many late-metal complexes have been prepared which activate hydrocarbons, but linking this reactivity with dioxygen reduction to achieve catalytic selective hydrocarbon oxidation remains a challenge.[53] In these and other organometallic systems, the inertness of its supporting ligands and its reluctance to undergo outer-sphere electron transfer may make trimesityliridium a more attractive cooxidant than, say, copper salts. Second, the analysis presented here highlights some of the reasons for the reactivity of the $(mes)_3Ir{=}O/(mes)_3Ir$ couple toward oxygen atom transfer, notably the importance of minimizing inner-sphere reorganization energy. The use of these principles may aid in the development of new, perhaps cheaper or more reactive, oxygen atom transfer agents for use in catalysis.

Conclusions

Oxotrimesityliridium(V), $(mes)_3Ir{=}O$, undergoes degenerate oxygen atom transfer with trimesityliridium(III), $(mes)_3Ir$, at unprecedentedly fast rates ($k_{IrIr} = 5 \times 10^7\ M^{-1}\ s^{-1}$, extrapolated to 293 K). In contrast, the osmium(VIII) oxo complex $(ArN)_3Os{=}O$, with an essentially identical metal−oxygen bond strength, transfers its oxygen to $(ArN)_3Os$ 12 orders of magnitude more slowly ($k_{OsOs} = 1.8 \times 10^{-5}\ M^{-1}\ s^{-1}$). Cross-reaction takes place at intermediate rates, in quantitative agreement with a Marcus-type analysis. The unusual facility of the iridium oxygen atom transfer can be explained by orbital alignment (both the HOMO of $(mes)_3Ir$ and the LUMO of $(mes)_3Ir{=}O$ have σ symmetry, making atom transfer allowed in a linear geometry) and by low inner-sphere reorganization energy (the triaryliridium geometry is structurally identical in the III, IV, and V oxidation states). The ability of $(mes)_3Ir$ to activate dioxygen and then transfer an oxygen atom to another metal has been demonstrated in catalytic cycles involving osmium complexes as the substrate-activating species to achieve alkene and alcohol oxidation.

Acknowledgment. We thank Dr. Alicia Beatty for her assistance with the X-ray crystallography, Dr. Bill Boggess for his assistance with the mass spectra, and Dr. Doug Miller for his assistance with the low-temperature optical spectroscopy experiments. The Center for Research Computing at the University of Notre Dame provided computing resources for the electronic structure calculations. Financial support from the Camille and Henry Dreyfus Foundation (New Professor Award), DuPont (Young Professor Award), and the Dow Chemical Company (Innovation Recognition Program) is gratefully acknowledged. L.P. thanks the Bayer Corporation for a postdoctoral fellowship, administered by the Notre Dame Center for Environmental Science and Technology. S.B.S. thanks the Clare Boothe Luce Foundation and the National Science Foundation for graduate fellowships.

Supporting Information Available: Complete refs 22 and 23; variable-temperature NMR spectra of $(mes)_3Ir{=}O$; Eyring plots of bond rotation in $(mes)_3Ir{=}O$, dissociation of $(mes)_3Ir{-}O{-}Ir(mes)_3$, deoxygenation of $(ArN)_3Os{=}O$ by PPh_3, and oxygen atom transfer from $(mes)_3Ir{=}O$ to $Os(NAr)_3$; van't Hoff plot of oxygen atom transfer from $(mes)_3Ir{=}O$ to $Os(NAr)_3$; kinetic traces for oxygen atom transfer between $(ArN)_3OsO$ and $(Ar_DN)_3Os$ and for $(mes)_3IrO$/(quinuclidine)OsO_4-cocatalyzed air oxidation of octene; Cartesian coordinates, energies, and thermal corrections of all optimized structures; and a plot of energy vs distance scan for $(CH_3N)_3Os{-}O{-}Os(NCH_3)_3$ (PDF format); and crystallographic data for $(Me_2C_6H_3)_3Ir{-}O{-}Ir(C_6H_3Me_2)_3{\cdot}CD_2Cl_2$ in CIF format. This material is available free of charge via the Internet at http://pubs.acs.org.

JA065713H

(53) (a) Rostovtsev, V. V.; Henling, L. M.; Labinger, J. A.; Bercaw, J. E. *Inorg. Chem.* **2002**, *41*, 3608−3619. (b) Ackerman, L. J.; Sadighi, J. P.; Kurtz, D. M.; Labinger, J. A.; Bercaw, J. E. *Organometallics* **2003**, *22*, 3884−3890. (c) Vedernikov, A. N.; Binfield, S. A.; Zavalij, P. Y.; Khusnutdinova, J. R. *J. Am. Chem. Soc.* **2006**, *128*, 82−83.